JOURNAL OF SOLID STATE CHEMISTRY **132,** 389–393 (1997)
ARTICLE NO. SC977478

Structure and Electrical Conductivity of $AgTaS_3$

Changkeun Kim,* Hoseop Yun,*,[1] Youngju Lee,† Heekyoon Shin,† and Kwangkyoung Liou‡

** Department of Chemistry and † Department of Physics, Ajou University Suwon 442-749, Republic of Korea; and ‡ Department of Chemistry, Sun Moon University, Asan 337-840, Republic of Korea*

Received January 14, 1997; in revised form May 14, 1997; accepted May 21, 1997

Single crystals of the compound $AgTaS_3$ have been prepared through reactions of the elements with halide mixtures. The structure of $AgTaS_3$ has been analyzed by single-crystal X-ray diffraction methods. $AgTaS_3$ crystallizes in the space group D_{2h}^{17}–*Cmcm* of the orthorhombic system with four formula units in a cell of dimensions $a=3.378(2)$, $b=14.070(5)$, $c=7.756(3)$ Å. The structure of $AgTaS_3$ consists of two-dimensional $^2_\infty[TaS_3^-]$ layers separated by Ag^+ cations. The layer is composed of Ta-centered bicapped trigonal prisms stacked on top of each other by sharing triangular faces. These chains are linked to form the infinite two-dimensional $^2_\infty[TaS_3^-]$ slabs. These layers are held together through van der Waals interactions, and Ag^+ ions reside in the distorted octahedral sites between the layers. The temperature dependence of the electrical conductivity along the needle axis of $AgTaS_3$ shows the typical behavior of an extrinsic semiconductor. © 1997 Academic Press

INTRODUCTION

Synthesis, crystal structure, and electrical conductivity of $AgTaS_3$ have been reported but with limited accuracy (1, 2). Single crystals with reasonable quality and size suitable for diffraction studies and physical properties measurements have not been obtained with traditional solid state synthetic techniques. Consequently, the X-ray diffraction data have been collected with powders and structural analysis has been carried out by the Rietveld profile refinement technique with the help of electron diffraction (2). In addition, the crystal structure of $AgTaS_3$ has been refined in the noncentrosymmetric, polar space group $Cmc2_1$, and it has been suggested that it should be described in the centrosymmetric space group *Cmcm* (3). As would be expected in such circumstances, the distances and angles reported previously are much less regular than those found in other similar compounds (4).

The compound $AgTaS_3$ possesses physical and structural features that may aid in the understanding of other metal chacogenides with related structures. Metal chalcogenides including d^{10} ions such as Ag(I) and Cu(I) have been reported to exihibit remarkable low energy barriers among various coordinations. This is closely related to the occurrence of ionic conductivity and large anisotropic displacement parameters (ADP) (5, 6). Also, the trigonal prismatic chain composed of Ta and S atoms is similar to those of TaS_3 (7), which has been known for quasi-one-dimensional characters and two charge density wave (CDW) transitions depending on their subtle differences of the chain structures.

To prepare single crystals of metal chacogenides, eutectic halide mixtures were used as reactive fluxes. This synthetic technique appears to be of general utility in preparing crystalline chalcogenides (e.g., KNb_2PS_{10} (8), $Rb_3Yb_7Se_{12}$, $CsEr_3Se_5$ (9), $CaYbInQ_4$ (Q = S, Se) (10), $Ca_4(RE)_2In_4Q_{13}$ (RE = La, Nd, Sm, Gd; Q = S, Se) (11), and $ATiPS_5$ (A = K, Rb) (12)). The significance of $AgTaS_3$ has inevitably led us to reexamination of the synthesis, crystal structure, and electrical conductivity.

EXPERIMENTAL

Synthesis

Single crystals of $AgTaS_3$ were prepared by the reaction of elemental Ag, Ta, and S powders with the use of the reactive flux technique. Stoichiometric combinations of the pure elements, Ag powder (CERAC 99.999%), Ta powder (CERAC 99.9%), and S powder (Aldrich 99.999%) were loaded in a quartz tube and AgCl/LiCl eutectic mixture was added in a weight ratio of $AgTaS_3$:AgCl/LiCl = 1:6. The tube was evacuated to $\sim 10^{-2}$ Torr, sealed, and heated gradually (80°C/hr) to 630°C in a tube furnace, where it was kept for 3 days. The tube was slowly cooled to 300°C at 7°C/hr and quenched. Black shiny needle-shaped crystals up to 1.2 mm were found. The crystals appear to be stable in air. Electron microprobe analysis of the crystals confirmed the presence of all three elements in a ratio of approximately 1:1:3. Structural details of the compound were determined by a single-crystal X-ray diffraction study.

[1] To whom correspondence should be addressed.

0022-4596/97 $25.00

Crystallographic Studies

The crystal structures of $AgTaS_3$ were determined by single-crystal X-ray diffraction techniques. Preliminary examination and data collection were performed with Mo$K\alpha$ radiation ($\lambda = 0.7107$ Å) on an MXC3 diffractometer (Mac Science). Cell constants and an orientation matrix were determined from least-squares analysis, using setting angles of 22 reflections in the range $20.0^\circ < 2\theta < 28.0^\circ$ that had been automatically centered. The orthorhombic cell parameters and calculated volume are $a = 3.378(2)$, $b = 14.070(5)$, $c = 7.756(3)$ Å, $V = 368.6(3)$ Å^3. Additional crystallographic details are described in Table 1. Intensity data were collected with the ω–2θ scan technique. The intensities of two standard reflections, measured every 100 reflections, showed no significant deviations during the data collection. The systematic absences (hkl, $h + k = 2n + 1$; $h0l$, $l = 2n + 1$) are consistent with the orthorhombic space groups, D_{2h}^{17}–$Cmcm$, C_{2v}^{12}–$Cmc2_1$, and C_{2v}^{16}–$C2cm$. The centrosymmetric $Cmcm$ was assumed and satisfactory refinement confirmed the choice of the space group.

The initial positions for all atoms were obtained by using direct methods of the SHELXS-86 program (13). With the composition established, the data for $AgTaS_3$ were corrected for absorption with the use of the analytical method of Tompa and de Meulenaer (14). The structure was refined by full-matrix least-squares techniques with the use of the SHELXL-93 program (15). The final cycle of refinement performed on F_o^2 with 268 unique reflections afforded residuals w$R2 = 0.0770$ and conventional R index based on the reflections having $F_o^2 > 2\sigma(F_o^2)$ is 0.0287. A difference Fourier synthesis calculated with phase based on the final parameters shows no peak heights greater than 18.4% of that of a S atom. No unusual trends were found in the goodness of fit as a function of F_o, $\sin\theta/\lambda$, and Miller indices. Final values of the atomic coordinates and equivalent isotropic displacement parameters are given in Table 2. Anisotropic displacement parameters are given in Table 3.

TABLE 1
Details of X-Ray Data Collection and Refinement for $AgTaS_3$

Formula mass, amu	385.00
Space group	D_{2h}^{17}–$Cmcm$
a, Å	3.378(2)
b, Å	14.070(5)
c, Å	7.756(3)
V^a, Å^3	368.6(3)
Z	4
T, K	293(2)
Radiation	Graphite monochromated Mo$K\alpha$
Linear absorption coefficient, cm^{-1}	364.12
Transmission factor[b]	0.258–0.582
Density, calc. g/cm^3	6.937
Crystal size, mm^3	$0.44 \times 0.04 \times 0.015$
Scan type	ω–2θ
Scan speed, deg. min	5.0 in ω
Scan range, deg.	$1.2 + 0.35\tan\theta$
2θ limits, deg.	$3.0^\circ \le 2\theta \le 55.0^\circ$
Data collected	$+h$, $+k$, $+l$
No. of unique data with $F_o^2 > 0$	268
No. of unique data with $F_o^2 > 2\sigma(F_o^2)$	259
w$R2(F_o^2 > 0)$	0.0770
$R1$ (on F_o for $F_o^2 > 2\sigma(F_o^2)$)	0.0287
Goodness of fit on F^2	1.144
Min. and Max. residual e$^-$ density (e/Å^3)	−2.000 and 2.946

[a] α, β, and γ were constrained to be 90° in the refinement of cell constants
[b] The analytical method as employed in the Northwestern absorption program AGNOST

TABLE 2
Atomic Coordinates (×10^4) and Equivalent Isotropic Displacement Parameters (Å^2×10^3) for $AgTaS_3$

	x	y	z	U_{eq}[a]
Ag	0	0	5000	35(1)
Ta	0	2621(1)	2500	7(1)
S(1)	0	8956(3)	2500	8(1)
S(2)	0	6730(2)	4303(4)	8(1)

[a] U_{eq} is defined as one third of the trace of the orthogonalized U_{ij} tensor.

Conductivity Measurements

A single crystal of $AgTaS_3$ ($1.20 \times 0.04 \times 0.02$mm^3) was mounted with Ag paint on gold wires with copper extentions. The sample was put into a closed-cycle refrigerator in which the temperature was controlled between 10–300 K. A carbon–glass resistance thermometer was used with a Lake Shore DRC 91C controller for the temperature measurement. Resistance was measured by the ordinary dc four-probe method using a Keithley 181 nanovoltmeter and a Keithley 220 current source. To remove errors resulting from a possible offset, both directions of the current were measured and averaged.

TABLE 3
Anisotropic Displacement Parameters (Å^2×10^3) for $AgTaS_3$

	U_{11}	U_{22}	U_{33}	U_{23}	U_{13}	U_{12}
Ag	52(1)	26(1)	28(1)	− 18(1)	0	0
Ta	7(1)	8(1)	5(1)	0	0	0
S(1)	11(2)	7(2)	7(2)	0	0	0
S(2)	8(1)	12(1)	5(1)	0(1)	0	0

Note. The anisotropic displacement factor exponent takes the form

$$-2\pi^2[h^2a^{*2}U_{11} + k^2b^{*2}U_{22} + l^2c^{*2}U_{33} + 2klb^*c^*U_{23} + 2hla^*c^*U_{13} + 2hka^*b^*U_{12}]$$

RESULTS AND DISCUSSION

The general features of the structure of $AgTaS_3$ are the same as previously reported with the polar space group $Cmc2_1$ (2). This structural type can be found in the known chalcogenides, $FeUS_3$ (16) and antitype Pd_3Te_2 (17). Selected bond distances for $AgTaS_3$ are listed in Table 4. A view down the **a** axis, given in Fig. 1, shows the labeling scheme and the layer stacking. The structure of $AgTaS_3$ consists of $^2_\infty[TaS_3^-]$ layers separated by Ag^+ cations. The layer is composed of Ta-centered bicapped trigonal prisms stacked on top of each other by sharing triangular faces. These chains are parallel to the **a** axis and are also linked together to form slabs parallel to the **ac** plane. The capping Ta–S distance is slightly longer than the usual Ta–S distances. These slabs are held together through van der Waals interactions, and Ag^+ ions reside in the octahedral sites between the slabs. The prism base exhibits a shorter S–S distance (2.796(6) Å) compared to others (3.430(5) Å) and each face of the prism could be classified as an isosceles triangle. The longer distances correspond to the usual van der Waals distances between S atoms. The shorter S–S distance is much longer than the typical S–S distance in the anion S_2^{2-} (18) but remains smaller than the usual contacting distance. This prismatic chain is isostructural with the type II chain of monoclinic TaS_3 (7). The S–S distance in the type II chain of TaS_3 is 2.835 (3) Å and the larger distances are 3.389 (3) and 3.392 (4) Å. Only the type I and III chains with shorter $(S–S)^{2-}$ distances in TaS_3 are believed to be responsible for the two different charge density wave (CDW) transitions (19, 20).

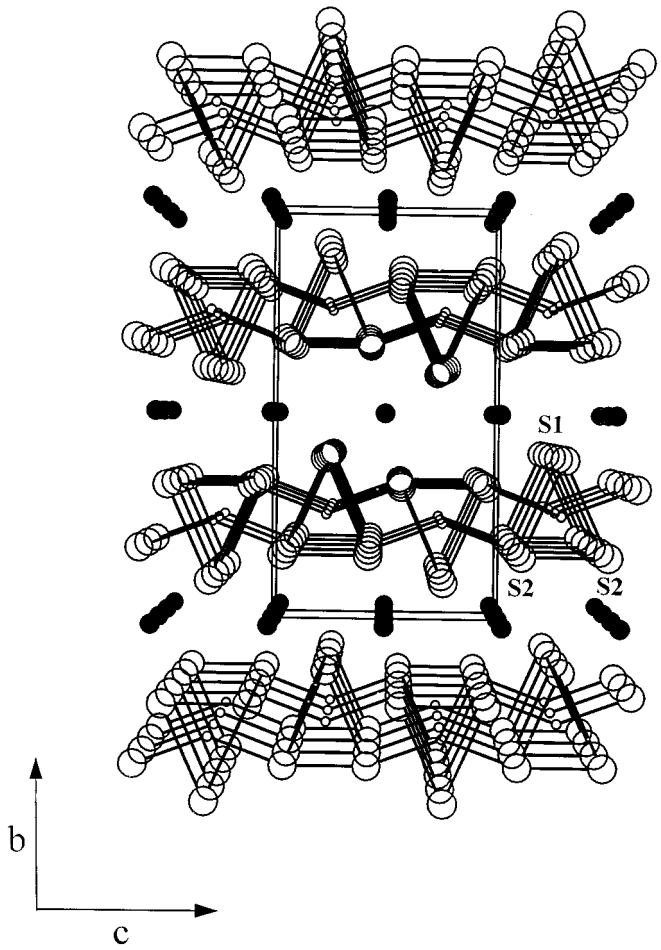

FIG. 1. A view down the **a** axis showing the labeling scheme and layer stacking. Open small circles are Ta atoms, filled circles are Ag atoms, and large open circles are S atoms.

TABLE 4
Bond Distances (Å) for $AgTaS_3$

Ag–S(1)#1	2.432(3)	Ag–S(1)#2	2.432(3)
Ag–S(2)#3	3.011(3)	Ag–S(2)#4	3.011(3)
Ag–S(2)#5	3.011(3)	Ag–S(2)#6	3.011(3)
Ag–Ag#7	3.378(2)	Ag–Ag#8	3.378(2)
Ag–Ag#9	3.878(2)	Ag–Ag#10	3.878(2)
S(1)–S(2)#4	3.430(5)	S(1)–S(2)#7	3.430(5)
S(2)–S(2)#8	2.796(6)		
Ta–S(1)#4	2.526(3)	Ta–S(1)#6	2.526(3)
Ta–S(2)#11	2.526(2)	Ta–S(2)#4	2.526(2)
Ta–S(2)#6	2.526(2)	Ta–S(2)#12	2.526(2)
Ta–S(2)#1	2.643(3)	Ta–S(2)#13	2.643(3)

Note. Symmetry transformations used to generate equivalent atoms:

#1 $-x, -y+1, -z+1$	#2 $x, y-1, z$
#3 $-x-1/2, -y+1/2, -z+1$	#4 $x+1/2, y-1/2, z$
#5 $-x+1/2, -y+1/2, -z+1$	#6 $x-1/2, y-1/2, z$
#7 $x+1, y, z$	#8 $x-1, y, z$
#9 $-x, -y, z+1/2$	#10 $-x, -y, z-1/2$
#11 $x-1/2, y-1/2, -z+1/2$	#12 $x+1/2, y-1/2, -z+1/2$
#13 $-x, -y+1, z-1/2$.	

The coordination around Ag atom can be described as [2 + 4] bonding interactions (Fig. 2). Four S atoms are bound to the Ag atoms in the plane (3.011(3) Å), whereas two trans S atoms are coordinated to the Ag atom (2.432(3) Å). These values are comparable to the sum of the ionic radii of each element (2.51 Å for CN = 2; 2.99 Å for CN = 6) (21). The distances and angles found here are much more regular than those found previously (2). For example, their equatorial Ag–S distances range from 2.81(2) to 3.20(3) Å compared with 3.011(3) Å here. We note that Ag exhibits extraordinarily large anisotropic displacement parameters. This is a common trend of d^{10} elements such as Ag(I) and Cu(I). The reason for this high displacement motion could be explained by the second-order Jahn–Teller coupling between the filled silver e_g manifold and the empty *s* orbitals, where the distortion from the ideal octahedron keeps the 4-fold rotation symmetry (22). According to the calculations conducted by Burdett et al., tetragonal contraction would be favored for the d^{10} configuration (5) and this is compatible with our results.

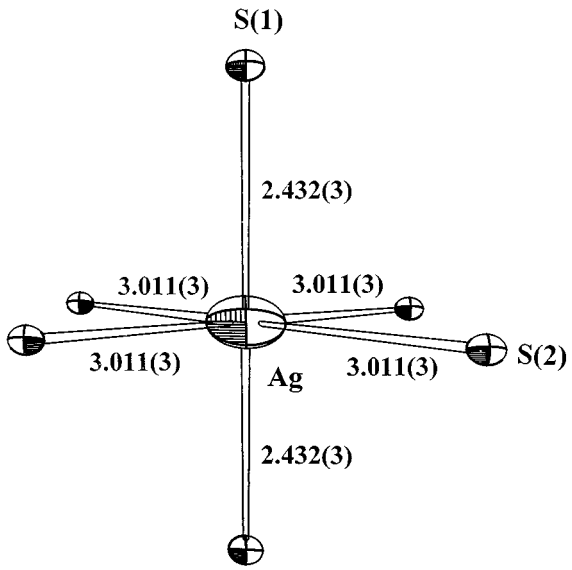

FIG. 2. Coordination geometry around the Ag atom in the $AgTaS_3$ structure with the labeling scheme. Distances are shown in Å.

The temperature dependence of the conductivity (σ) along the needle axis **a** shows a typical behavior of an extrinsic semiconductor (23). No signs of the CDW transition have been detected. These results are consistent with the simple classical valence description $Ag^{+}Ta^{5+}(S^{2-})_3$. A plot of the conductivity as a function of temperature is shown in Fig. 3. Also shown in the inset of Fig. 3 is $\ln\sigma$ vs $1/T$ in the temperature range of $T \geq 60$ K. Near room temperature it shows some evidence of intrinsic activation. Although there are only 2–3 data points in this intrinsic region it is not difficult to estimate $\sim 10^{-2}$ eV of activation energy which is comparable with the previously reported value (6×10^{-2} eV) obtained from sintered pellet. The conductivity increases as the temperature goes down to 100 K, which reflects the scattering of carriers with phonons in the extrinsic region. As the temperature is lowered further, dominant scattering is taken over by the impurity and the conductivity begins to fall. At even lower temperatures ($T < 60$ K) a freeze-out region is approached where the thermal energy becomes small compared to the carrier excitation energy. In this region, charge carriers are energetically localized near the impurity site and the only relevant conduction is due to thermal energy assisted by hopping. It is well known that the hopping conduction changes its mechanism from the nearest neighbor to the variable range hopping (VRH) as the hopping energy becomes small (24). Thus, VRH is expected at very low temperatures. The solid line in the figure is the fit by the formula $\sigma = \sigma_1 \cdot \exp\{-(1/T)\} + \sigma_2 \cdot \exp\{-(1/T)^{1/2}\}$, which signifies the conduction mixed by the nearest neighbor and the VRH. If this fitting is acceptable it implies that the low temperature limit of our measurement is not enough for the sample to show a pure VRH but in the middle of the change over to the VRH.

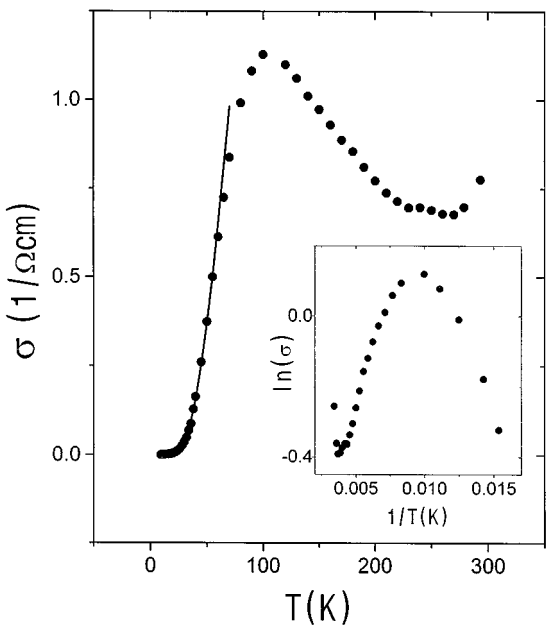

FIG. 3. Plot of the conductivity (σ) of $AgTaS_3$ vs temperature. Inset: plot of $\ln\sigma$ vs $1/T$ in the temperature range of $T \geq 60$ K.

ACKNOWLEDGMENTS

This research was supported by the Korean Science and Engineering Foundation (KOSEF 961-0306-059-1). Financial support for the single-crystal X-ray diffractometer by the Ajou University Research Fund is gratefully acknowledged.

REFERENCES

1. H. Wada and M. Onoda, *Chem. Lett.*, 705 (1990).
2. H. Wada, M. Onoda, and H. Nozaki, *J. Solid State Chem.* **97,** 29 (1992).
3. R. E. Marsh, *J. Solid State Chem.* **102,** 283 (1993).
4. S. A. Sunshine and J. A. Ibers, *Acta Crystallogr. Sect. C* **43,** 1019 (1987).
5. J. K. Burdett and O. Eisenstein, *Inorg. Chem.* **31**(10), 1758 (1992).
6. R. A. Huggins, "Diffusion in Solids" (A. S. Nowick and J. J. Burton, Eds.). Academic Press, New York, 1975.
7. A. Meerschaut, L, Guemas, and J. Rouxel, *J. Solid State Chem.* **36,** 118 (1981).
8. J. Do and H. Yun, *Inorg. Chem.* **35**(13), 3729(1996).
9. S. Kim, S. Park, H. Yun, and J. Do, *Inorg. Chem.* **35**(18), 5283 (1996).
10. J. D. Carpenter and S. Hwu, *Chem. Mater.* **4,** 1368 (1992).
11. J. D. Carpenter and S. Hwu, *Inorg. Chem.* **34**(18), 4647(1995).
12. J. Do, K. Lee and H. Yun, *J. Solid State Chem.* **125,** 30 (1996).
13. G. M. Sheldrick, *Acta Crystallogr. Sect. A* **46,** 467 (1990).
14. J. de Meulenaer and H. Tompa, *Acta Crystallogr.* **19,** 1014 (1965).
15. G. M. Sheldrick, "SHELXL-93, Program for the Refinement of Crystal Structures." University of Göttingen, 1993.
16. H. Noël and J. Padiou, *Acta Crystallogr. Sect. B* **32,** 1593 (1976).

17. P. Matkovic and K. Schubert, *J. Less-Common Met.* **52,** 217 (1977).
18. A. F. Wells, "Structural Inorganic Chemistry," 5th ed. Clarendon, Oxford, 1984.
19. J. Ren and M.-H. Whangbo, *Phys. Rev. B* **46**(8), 4917 (1992).
20. E.. Canadell, I. E.-I. Rachidi, J. P. Pouget, P. Gressier, A. Meerschaut, J. Rouxel, D. Jung, M. Evain, and M.-H. Whangbo, *Inorg. Chem.* **29**(7), 1401 (1990).
21. R. D. Shannon, *Acta Crystallogr. Sect. A* **32**, 751 (1976).
22. S. Lee, P. Colombet, G. Ouvrard, and R. Brec, *Inorg. Chem.* **27**(7), 1291 (1988).
23. F. F. Y. Wang, "Introduction to Solid State Electronics." Elsevier, Amsterdam, 1980.
24. N. F. Mott and E. A. Davis, "Electronic Processes in Non-crystalline Materials". Oxford Univ. Press, Oxford, 1979.